Melt Blowing: General Equation Development and Experimental Verification

A model has been developed for steady polymer melt blowing. This model includes the dominant effect that the forwarding air has upon the process. Inertial, gravitational and heat transfer effects are also included. The model equations are solved numerically with both Newtonian and viscoelastic (Phan-Thien and Tanner) constitutive equations. The predicted results compare favorably with actual experimental data.

Marc A. J. Uyttendaele
Robert L. Shambaugh
Department of Chemical Engineering
and Materials Science
University of Oklahoma
Norman, OK 73019

Introduction

The melt blowing process is commercially important in the manufacture of thermoplastic fibers with diameters as small as 0.5 micron. In the melt blowing process (see Figure 1), a molten stream of polymer is extruded into a high-velocity stream of forwarding gas. The force of the gas rapidly attenuates the fiber from the approximately 500 micron diameter at the capillary down to final fiber diameters that can be as small as 0.5 micron. This is a 1,000 X reduction in diameter and 1,000,000 X reduction in cross-sectional area.

The primary difference between melt blowing and conventional melt spinning (see Figure 2) is that a draw roll, rather than a gas stream, provides the attenuating force in melt spinning. In melt spinning, the gas into which the fiber is spun not only exerts a drag force on the filament but also cools the filament. In contrast, the gas used in melt blowing provides a substantial forwarding force and, because the gas is heated approximately to the polymer temperature, the gas prevents polymer solidification at distances close to the melt blowing die. Lack of a draw roll permits melt blowing at very high speeds: 30,000 m/min is possible with any common melt blowing head, while commercial melt spinning operations run at $\leq$3,200 m/min. Researchers in high-speed melt spinning have achieved, with difficulty, speeds of 7,000–12,000 m/min (Ziabicki and Kawai, 1985). Special, high-performance mechanical windups are required for this research.

Historically, work on melt blowing dates back to Wente's work at the Naval Research Laboratory (Wente, 1954, 1956). The technical aspects of melt blowing have been discussed very little except in patents (Buntin, 1974; Schwarz, 1983; McAmish, 1986). A recent article by Shambaugh (1988) gives an overview of the melt blowing process.

Since melt blowing has much in common with conventional melt spinning, a brief review of the literature on melt spinning is in order. Though melt spinning was developed commercially by Du Pont in the 1930's, only in the last 25 years have mathematical models been developed for melt spinning. Ziabicki and Kedzierska (1960, 1961), Ziabicki (1961), Kase and Matsuo (1965), and Matovich and Pearson (1969) developed the basic momentum, continuity, and energy balances that apply to a spinning threadline. They, however, applied these equations only to low-molecular-weight, inelastic liquids. Since most real polymers have material properties that are highly dependent on deformation rate, Fisher and Denn (1976) extended previous work to include polymers with a power law viscosity and a constant shear modulus. Gagon and Denn (1981) modeled the melt spinning of a visoelastic fluid with the inclusion of heat transfer, inertial and air drag effects. Their model agrees well with experimental data for the spinning of poly(ethylene terephthalate) at commercial speeds of 1,000–4,000 m/min. Excellent overviews are available on melt spinning (Ziabicki, 1976), on elongational flow (Petrie, 1979), and on high-speed spinning (Ziabicki and Kawai, 1985). Recent articles indicate that melt spinning continues to be an area of active research (Papanastasiou et al., 1987; Schultz, 1987; Lu and Spruiell, 1987).

Model Formulation

As has been done in the past for melt spinning, we will assume that the momentum and mass conservation equations can be averaged over the fiber cross-section. Also, these averaged equations will be assumed accurate at locations beyond the die swell: a melt blown fiber, like a conventional melt spun fiber, exhibits a die swell near the spinneret. We will write continuity, momentum and energy equations for the fiber spinline only. The surrounding gas conditions (velocity and temperature) will be considered as given functions of axial position and, thus, will enter as boundary conditions into the solution of the spinline equations.

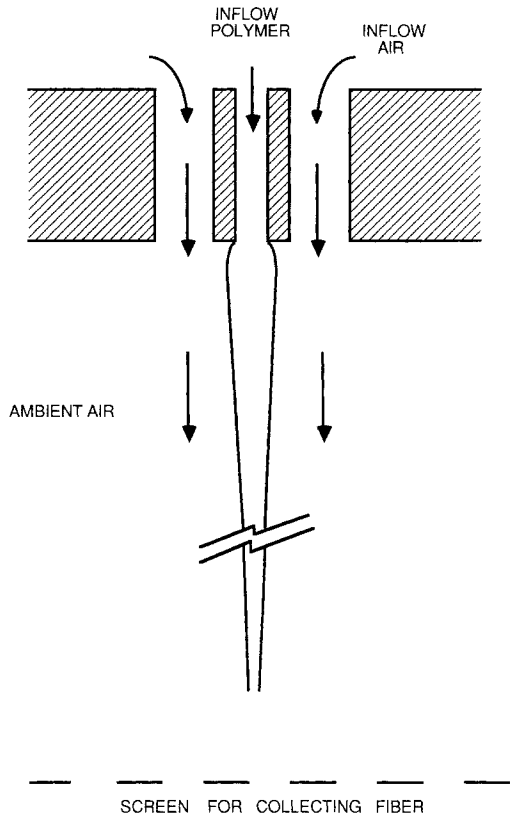

Figure 1. Melt blowing process.

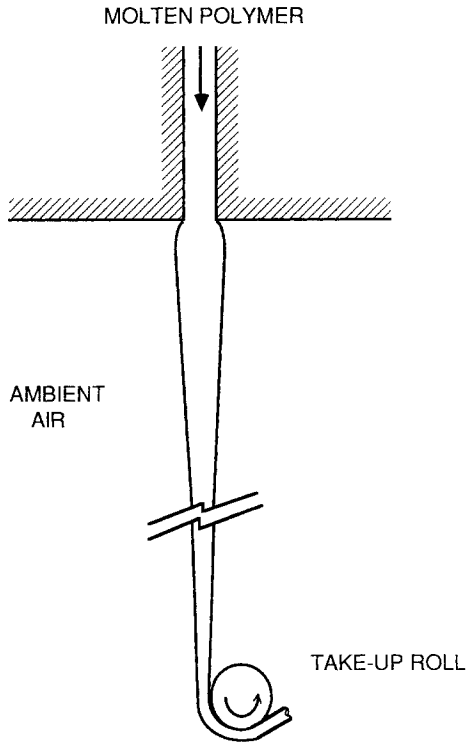

Figure 2. Conventional melt spinning.

The melt blowing process has three regions of operation (Shambaugh, 1988). In region I, the low gas velocity region, the fibers are continuous and the final fiber diameters are ≥ 10 micron. In regions II and III, fiber breakage and various instabilities occur. We will confine our work in this paper to an analysis of region I.

Continuity and momentum equations

The application of the continuity equation to the spinline gives:

$$A_z v_{fz} = Q = \text{constant} \tag{1}$$

where

A_z = fiber cross-sectional area
v_{fz} = axial fiber velocity
Q = volumetric polymer flow rate

Implicit in Eq. 1 is the constancy of polymer density. Essentially all previous workers on melt spinning have made this approximation. The assumption is not inaccurate: polymer density changes only about 10% between the molten state at spinneret temperatures and the solidification point. Perhaps more importantly, inclusion of variable density greatly increases the complexity of the spinning equations.

The differential form of the momentum equation is

$$\frac{d}{dz}\left[\pi \frac{d_z^2}{4}(\tau^{zz} - \tau^{xx})\right] = j\pi d_z C_f \rho_a \frac{v_{\text{rel}}^2}{2} + \rho_f Q \frac{dv_{fz}}{dz} - \frac{\pi d_z^2}{4}\rho_f g \tag{2}$$

where

z = axial position
τ^{zz}, τ^{xx} = components of the extra stress in the spinning and transverse directions, respectively
C_f = air drag coefficient
ρ_a = air density
v_{rel} = difference in velocity between the filament and forwarding air
ρ_f = polymer density
d_z = fiber diameter
g = gravitational acceleration

The j factor accounts for the fact that, near the spinneret, the gas exerts a positive (downward) force on the filament, but further down the threadline the force exerted by the gas is negative. The j is negative when $v_{az} > v_{fz}$ and positive when $v_{az} < v_{fz}$.

The drag coefficient C_f was correlated by Matsui (1976) with the relation

$$C_f = \beta(Re_{\text{rel}})^{-n} \tag{3}$$

where Re_{rel} is the air Reynolds number. Matsui developed his correlation for melt spinning speeds up to 6,000 m/min. Matsui's correlation has been extended to melt blowing speeds up to 30,000 m/min (Narasimhan and Shambaugh, 1986). For melt blowing, we define Re_{rel} as

$$Re_{\text{rel}} = \frac{d_z |v_{\text{rel}}|}{\nu_{az}} \tag{4}$$

where $v_{rel} = v_{az} - v_{fz}$. This definition of v_{rel} implies that, along the spinline, there is only a vertical component of the air velocity. This is a reasonable assumption because of the symmetry of air discharge about the spinneret. Note that v_{rel} is positive when the air is moving faster than the filament.

Energy equation

To estimate a convective heat transfer coefficient, we use the correlation

$$Nu_z = \gamma(Re_{rel})^m \tag{5}$$

This relation was developed by Kase and Matsuo (1965) for the parallel flow of gas along a cylinder. To simplify the conservation of energy equation, we assume steady state, no conductive resistance in the radial direction, no conduction in the axial direction, and no viscous dissipation. Then the equation of energy is simply

$$\rho_f C_{pf} v_{fz} \frac{dT_{fz}}{dz} = -\frac{4h_z}{d_z}(T_{fz} - T_{az}) \tag{6}$$

where

h_z = convective heat transfer coefficient
T_{fz} = filament temperature
T_{az} = air temperature
C_{pf} = heat capacity of the fiber

Constitutive equations

For a Newtonian fluid, the τ^{zz} and τ^{xx} components of the stress tensor are (Middleman, 1977)

$$\tau^{zz} = 2\eta \frac{dv_{fz}}{dz} \tag{7}$$

$$\tau^{xx} = -\eta \frac{dv_{fz}}{dz} \tag{8}$$

Equations 2, 6, 7 and 8 are the four equations that describe Newtonian, nonisothermal melt blowing.

The viscoelastic behavior of a polymer in an elongational flow field can be modeled with the following set of constitutive equations (Phan-Thien, 1978):

$$\tau^{zz} = \sum_i \tau_i^{zz} \tag{9}$$

$$\tau^{xx} = \sum_i \tau_i^{xx} \tag{10}$$

$$K_i \tau_i^{zz} + \lambda_i \left[v_{fz} \frac{d\tau_i^{zz}}{dz} - 2(1 - X)\tau_i^{zz} \frac{dv_{fz}}{dz} \right] = 2G_i \lambda_i \frac{dv_{fz}}{dz} \tag{11}$$

$$K_i \tau_i^{xx} + \lambda_i \left[v_{fz} \frac{d\tau_i^{xx}}{dz} + (1 - X)\tau_i^{xx} \frac{dv_{fz}}{dz} \right] = -G_i \lambda_i \frac{dv_{fz}}{dz} \tag{12}$$

where $i = 1, 2, 3, \ldots$

and

$$K_i = \exp\left[\frac{E}{G_i} (2\tau_i^{xx} + \tau_i^{zz}) \right] \tag{13}$$

These equations are derived from the application of the Phan-Thien and Tanner rheological model to a simple elongational flow. The Phan-Thien and Tanner model allows the use of a discrete spectrum of relaxation times. The factor X is a viscous shear thinning parameter, and E is a parameter related to stress saturation at high extension rates. When both parameters are set equal to zero, the common (upper convected) Maxwell fluid model is recovered.

Equations 2, 6, 11 and 12 describe the mechanical and thermal history of a viscoelastic fluid in the melt blowing process.

Experimental details

The experiments were carried out with a single hole melt blowing device similar to that shown in Figure 1. The spinneret capillary was 0.76 mm (0.030 in.) inside diameter with an L/D of 33. The gas annulus was concentric with the spinneret capillary. The annulus had a 1.27 mm (0.050 in.) inside diameter and a 2.38 mm (0.094 in.) outside diameter. The annulus length was 9.53 mm (0.374 in.), and the annulus cross-sectional area was constant over this length. Controlled polymer flow was provided by a 19.1-mm (¾-in.)-diameter Brabender extruder which fed a modified gear pump; pressures of 3.4×10^7 Pa (5,000 psi) and temperatures of 400°C were possible. A 7-kW electric heater provided gas at temperatures up to 650°C and pressures up to 6.9×10^5 Pa (100 psi).

Photographs of the spinline were taken online with a Canon 35 mm camera and high-speed flash system. Fiber diameters were determined by measurements on 20 cm × 25 cm (8 in. × 10 in.) prints; to correct for fiber motion (a problem when photographing small diameters), the photographs of the moving filaments were calibrated against photographs of stationary filaments. Off-line examination of the collected fibers was done with optical microscopy and scanning electron microscopy.

The melt blown fibers were collected as a mat upon a metal screen placed one meter below the spinneret. The polymer used in our experimental runs was 35 MFR (melt flow rate) DYPRO 3861 polypropylene donated by the Fina Company. This polypropylene has an $\overline{M}_w$ of 120,000 and an $\overline{M}_n$ of 30,000. At the operating temperatures used in melt blowing, the polymer undergoes some degradation. The extent of this degradation was determined from intrinsic viscosity measurements made on the collected fiber. The molecular weight was then determined from the Mark-Houwink relation

$$[\eta] = 0.000162[\overline{M}_w]^{0.77}$$

which was developed for polypropylene by Van Krevelin and Hoftyzer (1976). For the operating conditions used in our experiments, the polymer molecular weight ($\overline{M}_w$) decreased from 120,000 at the feed hopper to 100,000 at the spinneret; negligible degradation took place from the spinneret to the collection screen. The elongational viscosity of the degraded polymer was assumed proportional to the 3.5 power of $\overline{M}_w$ (Lu and Spruiell, 1987).

The zero shear rate viscosity of Fina Dypro 3861 polypropylene is 350 Pa · s at 230°C (Cooper, 1987). To permit estima-

tion of viscosity as a function of temperature, the zero shear rate viscosity was assumed to follow the Arrhenius-type relation (Tadmor and Gogos, 1979)

$$\eta_o = 350 \exp\left[\frac{\Delta E}{R}\left(\frac{503 - T}{503T}\right)\right]$$

where

ΔE = activation energy
R = gas constant
T = temperature, K

As suggested by Ziabicki (1976), a value of $\Delta E = 10.1$ kcal/mol was used for our polypropylene. This activation energy is closely bracketed by ΔE values from Tadmor and Gogos' data (1979) for commercial polypropylene: Exxon PP CD460 has $\Delta E = 11.4$ kcal/mol, while Union Carbide PP E612 has $\Delta E = 9.3$ kcal/mol. For the viscoelastic model, the assumed value of the elastic modulus G was 28 kPa; this G value is based on data taken by Tzoganakis et al. (1988) for polypropylene with $M_w/M_n = 4.49$ and $M_w = 195{,}000$. The Phan-Thien and Tanner parameters X and E were assumed to be 0.1 and 0.015, respectively. These values were originally determined for polystyrene (Phan-Thien, 1978), but these same values have been successfully used for other viscoelastic materials. For example, Phan-Thien (1978) used these values to describe polyethylene spinning (the viscoelastic behavior of polyethylene is similar to polypropylene). As will be discussed here, these estimated values of G, X and E are quite adequate for the prediction of melt blowing behavior: the model is not very sensitive to changes in these parameters.

Boundary conditions

In conventional melt spinning calculations, the speed of the takeup roll fixes the final velocity of the filament and hence provides a boundary condition which permits the solution of the model equations. An initial value of F_o is guessed, and an iteration procedure converges to the value of F_o which generates a solution that satisfies the specified takeup speed. (Other boundary conditions that must be satisfied include the initial filament velocity, the initial filament temperature, and the filament temperature at the freeze point.) Analogously, melt blowing may be modeled by the careful consideration of the forces acting on the filament both before and after the polymer stream solidifies. At some point along the threadline, the attenuation of the fiber becomes negligible; the polymer stream 'freezes.'

This freezing phenomenon does not necessarily occur at the usual T_g- or T_m-phase transition of the polymer melt. The freezing could be related to stress-induced crystallization, which is one of the most characteristic features of high-speed melt spinning (Ziabicki and Kawai, 1985). The freezing phenomenon could also be explained by the rapid increase of the elongational viscosity above a critical elongational deformation. This increase in elongational viscosity is due to a structural change in the polymer melt into a form in which the molecular orientation can easily be increased (Ishizuka et al., 1980). Beyond the 'freezing point,' the fiber diameter remains constant until the fiber is laid down on a collection screen. Two external forces act upon the frozen part of the polymer stream: the gravitational force and the air drag force. A force balance around the frozen part of the filament shows that the sum of the cumulative gravitational and air drag forces acting upon the frozen part of the fiber has to be equal to the rheological force inside the filament at the 'freezing point.' [Chung and Abdalla (1985) suggested a similar force balance for the case of a spinline dragged by an air jet.]

With the physics of the problem assumed to be as described above, the following procedure was used to solve the melt blowing problem:

Step 1. The position of the fiber freeze was specified. For the range of experiments described herein, specifying $z = 5$ cm gave both a good fit to the data and permitted the solution to converge (see step 2). The effect of selecting a different freeze position will be discussed later. Specification of a freeze position is essentially equivalent to specifying a freeze temperature.

Step 2. The value of the initial rheological force F_o was determined by iteration. The proper value of F_o must satisfy the force balance equality between the rheological force at the freeze point and the cumulative gravitational and air drag forces acting upon the frozen part of the filament.

Air velocity and temperature profiles

The gas velocities below the melt blowing head were measured with a fine, 0.45-mm-diameter pitot tube; see Figure 3. Because of the annular shape of the discharge orifice, the near field velocity drops almost linearly, while the velocity drops according to a power law at distances farther from the annulus. The temperatures of the gas streams were also measured. As a comparison of Figures 4 and 5 with Figure 3 shows, the temperature profiles are similar to the velocity profiles. The temperature measurements were taken with a fine, 0.51-mm-diameter thermocouple; the readings were corrected for the difference between stagnation and static temperatures. The functions listed on Figures 3–5 were used in the model to calculate v_{az} and T_{az} at axial positions along the filament.

Experimental results and model fit

Two case studies were conducted for the experimental verification of the computer model developed in this work. These studies are referred to as the "low gas velocity" and the "high gas velocity" experiments. Important parameters for the studies are listed in Table 1. For the drag force and heat transfer corre-

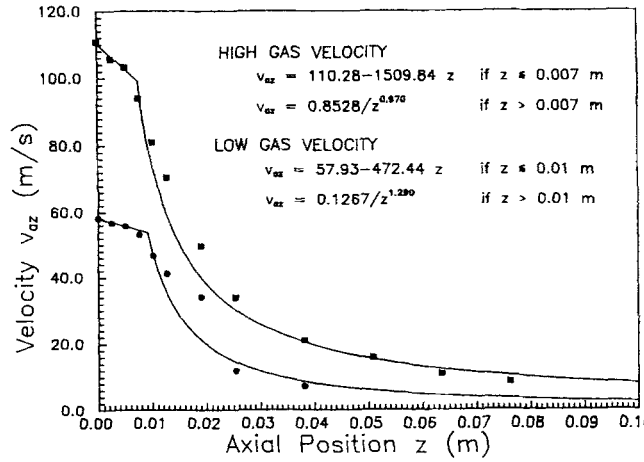

Figure 3. Velocity profiles of the annular air jet used in the melt-blowing experiments.

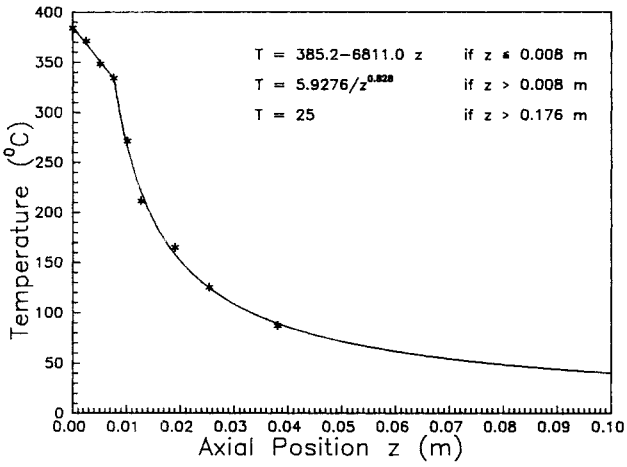

Figure 4. Temperature profile of the air jet used in the melt-blowing experiments.
This profile is for the low gas rate.

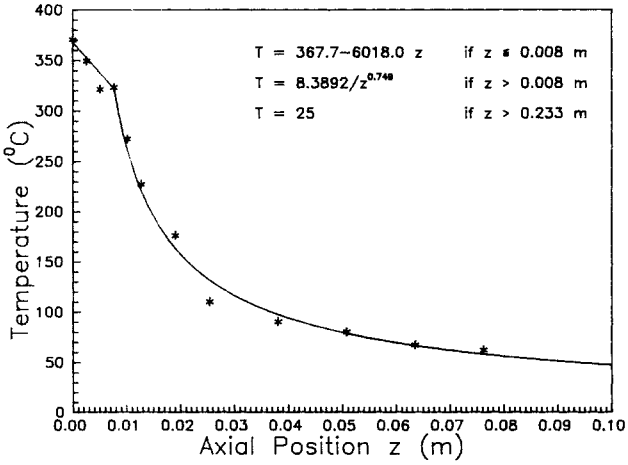

Figure 5. Temperature profile of the air jet used in the melt-blowing experiments.
This profile is for the high gas rate.

Table 1. Melt-Blowing Experiments

Starting Polymer: Fina Dypro 3861 35 MFR Polypropylene		
Polymer at Spinneret:	Conditions	
$\bar{M}_w$	100,000	
$\bar{M}_n$	30,000	
Temperature	310°C	
Throughput	10.983 mm³/s	
Spinneret Hole Diameter	0.762 mm	
Air annulus:		
Inside Diameter	1.270 mm	
Outside Diameter	2.388 mm	
Length	9.530 mm	
Air Conditions at Exit of Annulus:	Low Gas Rate Experiment	High Gas Rate Experiment
v_{ao}(m/s)	57.93	110.28
T_{ao}(°C)	385	368
Maximum Die Swell (μm)	960.6	949.0

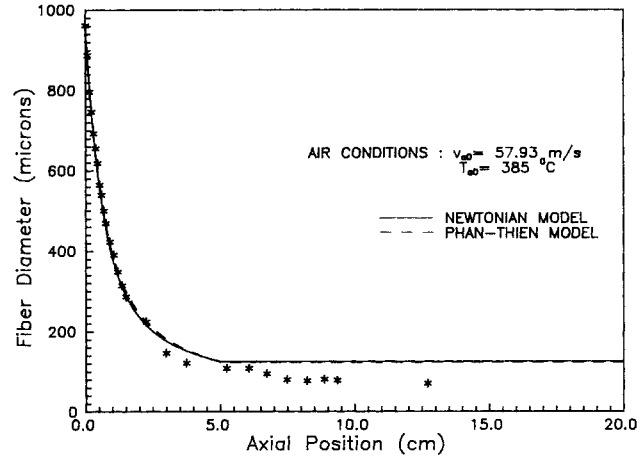

Figure 6. Melt-blowing data: Newtonian vs. Phan-Thien model.
This profile is for the low gas velocity.
For the Newtonian model, $F_o = 2.928 \times 10^{-4}$N, $d_f = 124.3$ μm, $T_f = 260$°C, and $F_{rheo,f} = 0.823 \times 10^{-4}$N.
For the Phan-Thien model, $F_o = 2.921 \times 10^{-4}$N, $d_f = 122.6$ μm, $T_f = 271$°C, and $F_{rheo,f} = 0.795 \times 10^{-4}$N.

lations (Eqs. 3 and 5), the assumed base values of β, n, γ and m were 0.37, 0.61, 0.42 and 0.334, respectively.

Figures 6 and 7 compare actual experimental data with the predictions of both the Newtonian model and the Phan-Thien and Tanner model. One relaxation time was used in the Phan-Thien and Tanner model. As previously discussed, a freeze point of 5 cm was used in the model predictions. Figure 6 concerns data and modeling for the low gas velocity. As the figure shows, the Newtonian predictions are almost the same as the predictions of the Phan-Thien and Tanner model. Up to the assumed freeze point, both models provide an excellent fit to the data. Beyond the freeze point, both model predictions are too high, though the Phan-Thien model's prediction is very slightly lower than the Newtonian model's prediction. In Figure 7, model predictions at the high gas velocity are compared with actual exper-

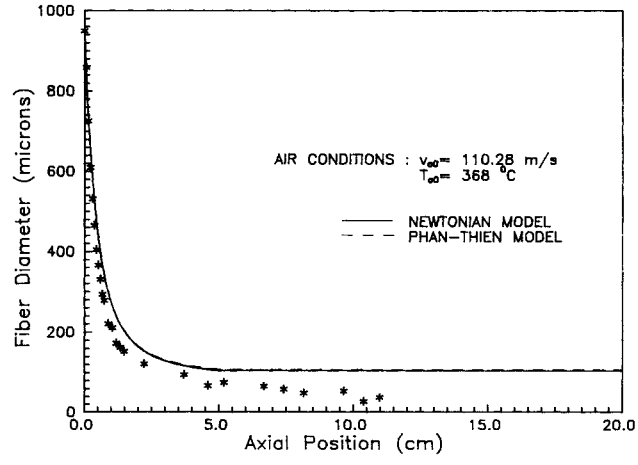

Figure 7. Same as Figure 6, except for the higher gas velocity.
For the Newtonian model, $F_o = 4.505 \times 10^{-4}$N, $d_f = 103.8$ μm, $T_f = 253$°C, and $F_{rheo,f} = 0.460 \times 10^{-4}$N.
For the Phan-Thien model, $F_o = 4.528 \times 10^{-4}$N, $d_f = 104.8$ μm, $T_f = 253$°C, and $F_{rheo,f} = 0.482 \times 10^{-4}$N.

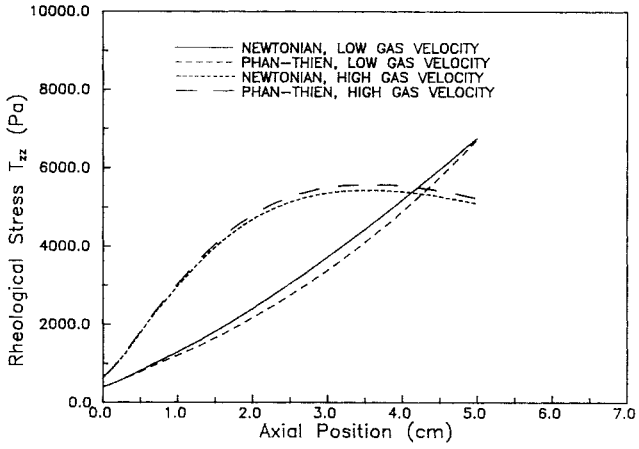

Figure 8. Stress growth predictions for the Newtonian and Phan-Thien models.
These growth curves correspond with Figures 6 and 7.

imental data. For Figure 7, the predicted diameters gradually become worse as axial position is increased from 0 to 5 cm. At 5 cm, the predicted diameters are about 20% high. Beyond 5 cm, the model predictions are about 100% high, just as they are in Figure 6. Also, the Newtonian model and Phan-Thien model predictions are nearly identical for the high gas rate.

Figure 8 shows the predicted stress growth along the fibers for both models and both gas rates. At the low gas velocity, the Newtonian and the Phan-Thien and Tanner models predict similar, monotonically increasing stresses as a function of axial position. For the high gas velocity, both models predict a maximum stress at about $z = 3.5$ cm.

Figure 9 shows the predicted fiber temperature profiles for both the low and high gas rates. Observe that, in the first 1 cm below the spinneret, the temperature of the polymer actually rises because the high velocity air is hotter than the polymer in this region. The gradient of the temperature change is about 1,400°C/m. This is almost four times as large as the approximately 380°C/m gradient of the predictions calculated by Gagon and Denn (1981) for high-speed melt spinning. The high-temperature gradient in melt blowing probably explains why the choice of constitutive equation is not that important: the temperature dependence of the viscosity is the dominant effect. Other

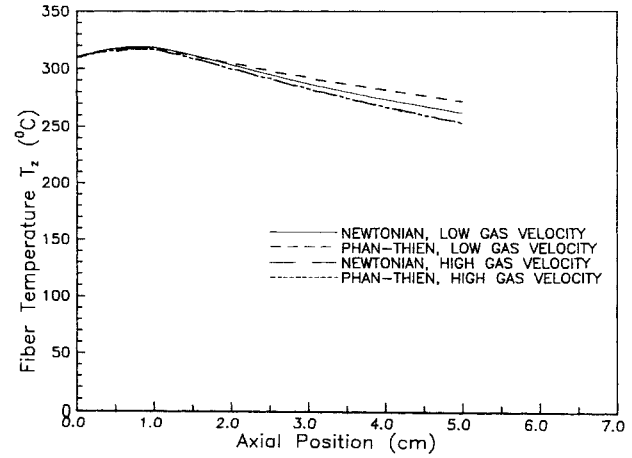

Figure 9. Predicted temperature profiles along the fiber.

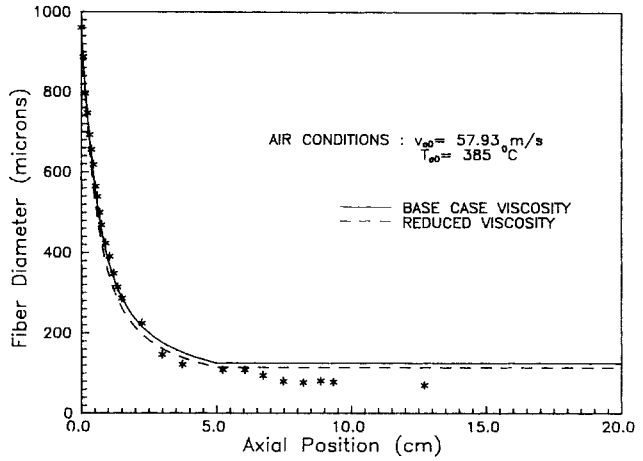

Figure 10. Effect of a 20% reduction in viscosity.
Calculations were done with the Newtonian model and the low gas rate.
For the reduced viscosity curve, $F_v = 2.646 \times 10^{-4}$N, $d_f = 113.7$ μm, $T_f = 260$°C, and $F_{rheo,f} = 0.650 \times 10^{-4}$N.

investigators (Ziabicki, 1976; Ziabicki and Kawai, 1985) have made similar observations about melt spinning. (And, as has just been stated, melt spinning has even less of a temperature gradient.)

Besides on-line measurement of fiber diameters (e.g., see the data points on Figure 6 and 7), off-line diameter measurements were made on the collected fibers. For the low and high gas rates, the average diameters determined by SEM were 57.7 and 41.5 μm, respectively. These numbers compare well with the on-line measurements.

Sensitivity to parameters

We now examine how sensitive the models are to the parameters. First, consider the effect of changing the viscosity in the simple (but effective) Newtonian model. If the viscosity is reduced 20%, we get the predictions shown in Figures 10 and 11. Figure 10, the low gas rate case, shows that a reduced viscosity gives a little worse prediction for distances less than about 2.5

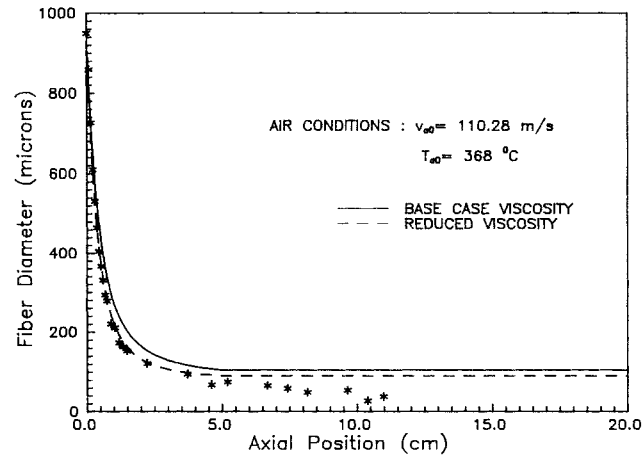

Figure 11. Same comparison as in Figure 10, except for the high gas rate.
For the reduced viscosity curve, $F_v = 3.912 \times 10^{-4}$N, $d_f = 89.7$ μm, $T_f = 256$°C, and $F_{rheo,f} = 0.187 \times 10^{-4}$N.

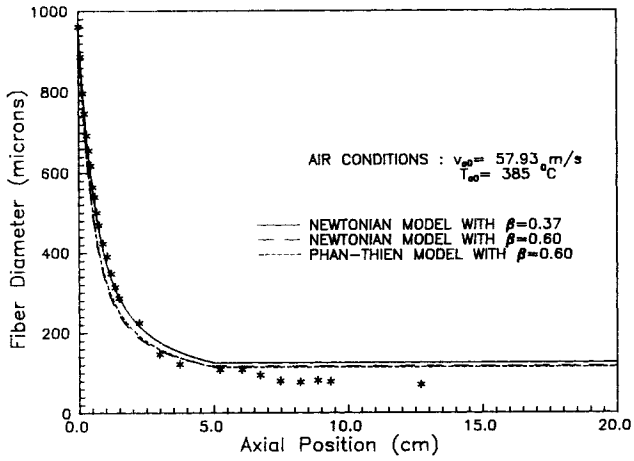

Figure 12. Effect of increased β in the Matsui correlation.

Calculations were done for the low gas rate.
For the Newtonian model with $\beta = 0.6$, $F_o = 3.610 \times 10^{-4}$N, $d_f = 115.8$ μm, $T_f = 262$°C, and $F_{\text{rheo},f} = 0.641 \times 10^{-4}$N.
For the Phan-Thien and Tanner model with $\beta = 0.6$, $F_o = 3.674 \times 10^{-4}$N, $d_f = 113.6$ μm, $T_f = 273$°C, and $F_{\text{rheo},f} = 0.637 \times 10^{-4}$N.
See Figure 6 for details on the calculations done with $\beta = 0.37$.

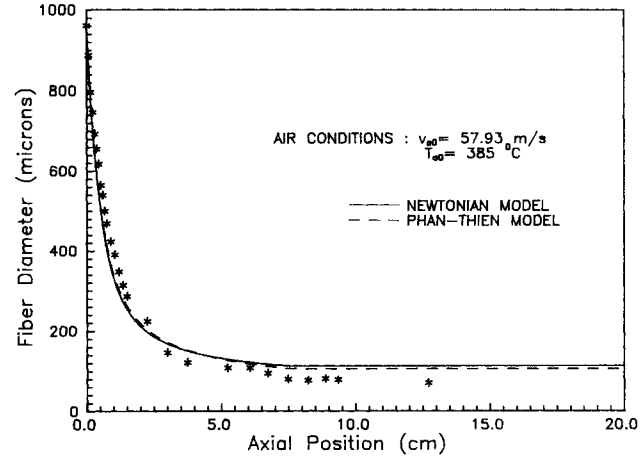

Figure 14. Simulation at low gas rate with an assumed freeze at 7.5 cm and $\beta = 0.60$.

For the Newtonian curve, $F_o = 3.610 \times 10^{-4}$N, $d_f = 111.6$ μm, $T_f = 238$°C, and $F_{\text{rheo},f} = 0.481 \times 10^{-4}$N.
For the Phan-Thien and Tanner curve, $F_o = 3.620 \times 10^{-4}$N, $d_f = 106.9$ μm, $T_f = 253$°C, and $F_{\text{rheo},f} = 0.470 \times 10^{-4}$N.

cm from the spinneret; for distances greater than 2.5 cm, the prediction is a little better. For the high gas rate case (Figure 11), the reduced viscosity curve is better for almost the entire profile.

Since air drag is of primary importance in the melt blowing process, the effect of varying the drag coefficient C_f is of great interest. Figure 12 shows that the predicted fiber attenuation is much more rapid when $\beta = 0.60$ (see Eq. 3) is used instead of $\beta = 0.37$. The fit is poorer for distances near the spinneret, but the final diameter prediction is improved. As with the $\beta = 0.37$ case (see Figure 6), there is little difference between the Newtonian and Phan-Thien and Tanner predictions. The results for the high gas rate case are shown in Figure 13. Here, the model predictions are substantially improved for the entire fiber profile. The β values of 0.37 and 0.60 are both well within the range of experimental values for β (Ziabicki, 1976).

Figures 14 and 15 show the effects of moving the assumed freeze point from $z = 5$ cm to $z = 7.5$ cm. For the low gas velocity (Figure 14), the prediction is slightly low for distances close to the spinneret, but the final predicted diameter is as good as any previous estimate. For Figure 15, the high velocity case, the predicted curves are excellent. Almost unnoticeable for these predictions is the characteristic discontinuity in the profile slope at the assumed freeze point.

Calculations were made with the heat transfer coefficient reduced by 25%. The resulting changes in predicted profiles were not large, see Figures 16 and 17.

Because of the closeness in the predictions of the Newtonian and Phan-Thien and Tanner models, one would not expect that changes in the viscoelastic model's parameters would cause

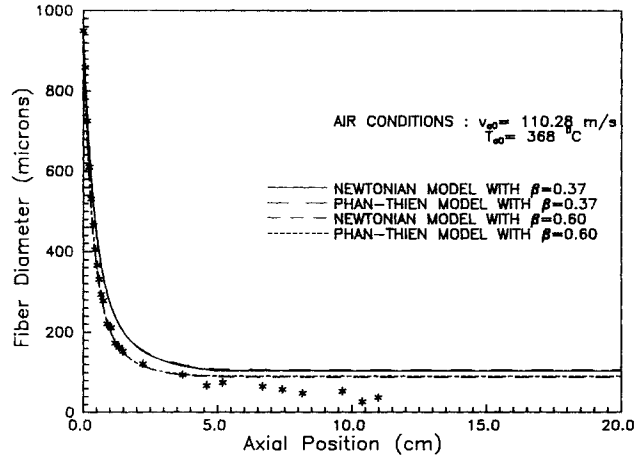

Figure 13. Same as Figure 12, but with calculations done for the high gas rate.

For the Newtonian model with $\beta = 0.60$, $F_o = 5.938 \times 10^{-4}$N, $d_f = 88.7$ μm, $T_f = 257$°C, and $F_{\text{rheo},f} = 0.124 \times 10^{-4}$N.
For the Phan-Thien and Tanner model with $\beta = 0.6$, $F = 5.998 \times 10^{-4}$N, $d_f = 89.5$ μm, $T_f = 257$°C, and $F_{\text{rheo},f} = 0.190 \times 10^{-4}$N.

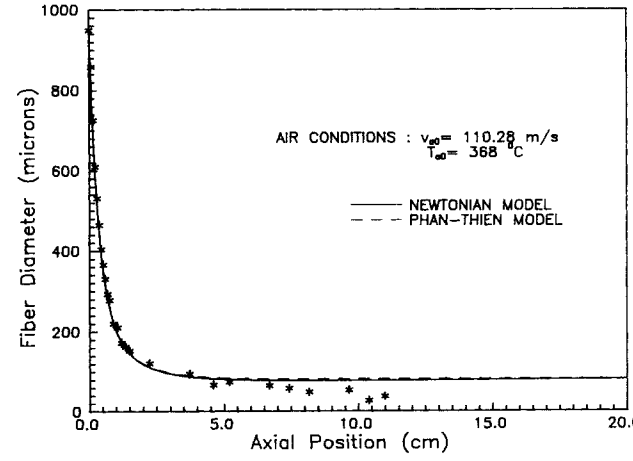

Figure 15. Simulation at high gas rate with an assumed freeze at 7.5 cm and $\beta = 0.60$.

For the Newtonian curve, $F_o = 5.970 \times 10^{-4}$N, $d_f = 77.7$ μm, $T_f = 231$°C, and $F_{\text{rheo},f} = 0.260 \times 10^{-4}$N.
For the Phan-Thien and Tanner curve, $F_o = 6.024 \times 10^{-4}$N, $d_f = 81.6$ μm, $T_f = 230$°C, and $F_{\text{rheo},f} = 0.505 \times 10^{-4}$N.

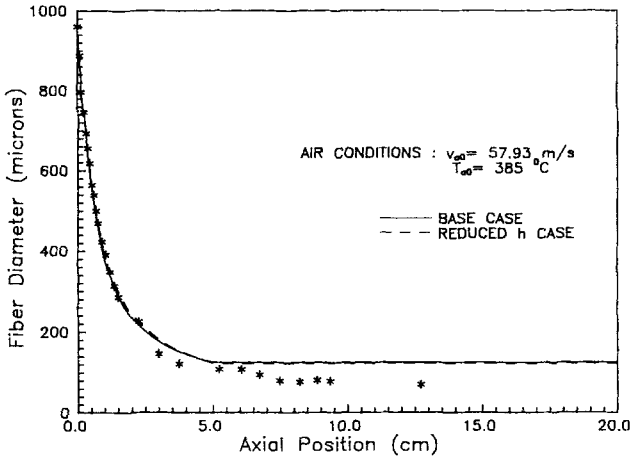

Figure 16. Effect of reducing the heat transfer coefficient.

Calculations were done at the low gas rate and with the Newtonian model.
See Figure 6 for details on the Newtonian base case.
The reduced h case, calculated with $\gamma = 0.315$, has $F_o = 2.920 \times 10^{-4}$N, $d_f = 122.2\ \mu$m, $T_f = 272$°C, and $F_{rheo,f} = 0.793 \times 10^{-4}$N.

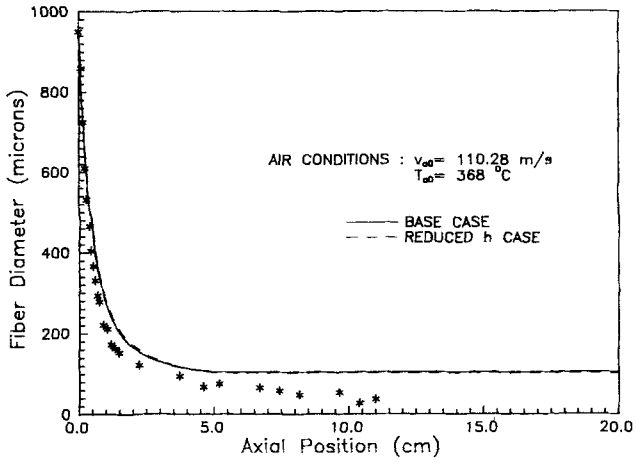

Figure 17. Same as Figure 16, except for the high gas rate.

See Figure 7 for details on the Newtonian base case.
The reduced h case has $F_o = 4.500 \times 10^{-4}$N, $d_f = 102.3\ \mu$m, $T_f = 265$°C, and $F_{rheo,f} = 0.438 \times 10^{-4}$N.

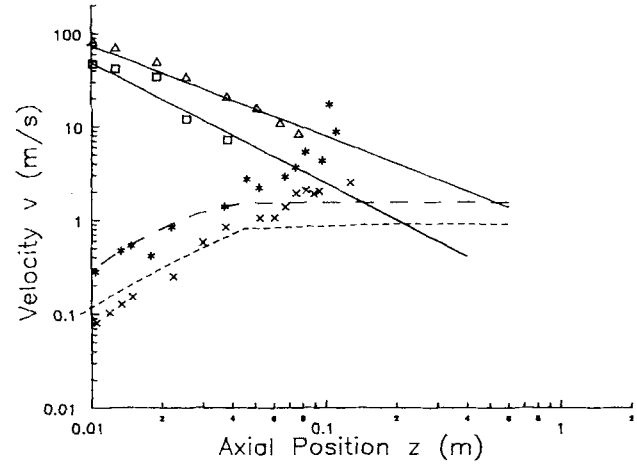

Figure 18. Comparison of gas and fiber velocities.

The upper two curves are gas velocities for the high (△) and low (□) gas velocities; the curves are correlations from Figure 3.
The lower two curves are fiber velocities correponding to the high gas velocity (*) and low gas velocity (x).
The data points on the lower two curves were calculated from measured fiber diameters and continuity.
The fiber velocity curves were predicted with a Newtonian assumption and $\beta = 0.60$.

large changes in the predictions. Indeed, this is what occurs; Table 2 shows the very minor effects of changing G, E, and X.

Figure 18 compares the velocity of the gas with the velocity of the filaments. Both experimental and predicted values of fiber velocities are included in the figure. At distances well below the spinneret (and beyond the assumed freeze point), the fiber velocity actually exceeds the gas velocity.

Figure 19 is a plot of the velocity gradient dv_{fz}/dz as a function of axial position. The figure includes gradients for the high and low gas rates and for the Newtonian and Phan-Thien models. The gradients were determined from the slopes of the model curves—i.e., from the predicted values of v_{fz}. The gradients are comparable to the 0–50 s^{-1} gradients observed in conventional melt spinning (Ziabicki, 1976).

For the low gas rate and the Newtonian model, the maximum gradient occurs at about 3 cm and stays large until the assumed freeze point of 5 cm is reached. The Phan-Thien prediction (at low gas rate) is similar, except that the maximum occurs right at 5 cm. For the high gas rate, both the Newtonian and the Phan-Thien models predict a maximum gradient at about 1.5 cm. A gradient curve with a maximum is a characteristic feature of

Table 2. Sensitivity of Phan-Thien and Tanner Model to Changes in Parameters

Conditions	Gas Rate	F_o(N)	d_f(μm)	T_f(°C)	$F_{rheo,f}$(N)
Base case (Fig. 6)	Low	2.921×10^{-4}	122.6	271	0.795×10^{-4}
G reduced by 25%	Low	2.923×10^{-4}	122.8	271	0.797×10^{-4}
$E = 0$	Low	2.921×10^{-4}	122.7	271	0.798×10^{-4}
$X = 0$	Low	2.924×10^{-4}	122.8	271	0.798×10^{-4}
$E = X = 0$ (Maxwell Model)	Low	2.924×10^{-4}	122.8	271	0.798×10^{-4}
Base case (Fig. 7)	High	4.528×10^{-4}	104.8	253	0.482×10^{-4}
$E = X = 0$ (Maxwell model)	High	4.533×10^{-4}	105.1	253	0.485×10^{-4}

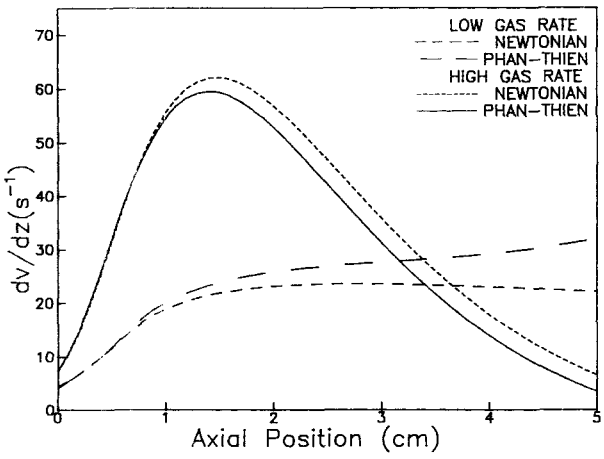

Figure 19. Velocity gradient along the threadline.
For all four cases, $\beta = 0.60$ and a freeze point of 5 cm were used.

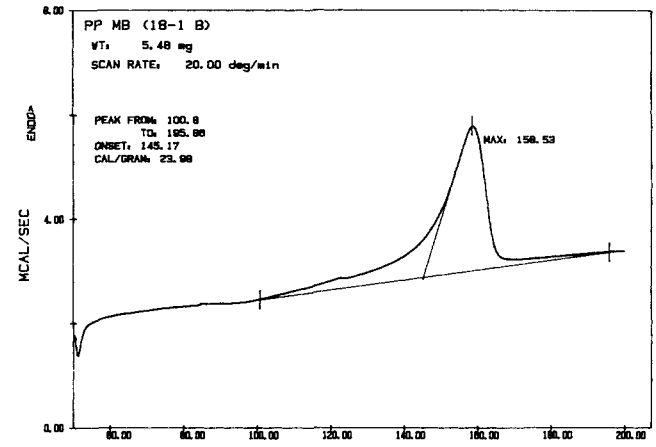

Figure 21. Typical DSC scan of melt-blown polypropylene.

melt spinning and is an indication of structural transition in the threadline (Ziabicki and Kedzierska, 1960; Ziabicki, 1976). The existence of maximum in our curves lends credence to our assumptions concerning solidification along the threadline.

Figure 20 is a plot of $(\lambda)(dv_{fz}/dz)$ for the Phan-Thien model and for both the low and high gas rates. As with the dv_{fz}/dz plots, the high gas rate case exhibits its maximum earlier than the low gas rate case (also compare Figure 8). The fact that the purely viscous (Newtonian) model does an adequate job of representing melt blowing is supported by the observation that $(\lambda)(dv_{fz}/dz) < 1$ over the range of both curves.

Crystallinity of melt blown fibers

Since our results imply that stress-induced crystallization plays a role in melt blowing, it was decided to analyze the crystallinities of the melt blown fibers. Crystallinities were determined with a DSC (differential scanning calorimeter).

The instrument we used was a Perkin-Elmer DSC-4. The temperature scale of the DSC was calibrated with an indium standard ($T_m = 156.6$°C). Jaffe (1981) suggests a scan rate of 20°C/min and a sample weight of 5–10 mg for DSC analysis of polymeric fibers. For this study, we used a 20°C/min scan rate and a 5–6 mg sample weight.

The preparation of fiber samples for reproducible results presents special problems in the DSC analysis of polymer fibers. Any deformation of the fiber during sample preparation must be avoided, since deformation will change the fiber's microstructure and alter its crystalline properties. The sample must be packed such that the sample maintains good thermal contact with the pan bottom. In the analysis of polyethylene fibers, several investigators (Clements et al., 1979; Smook and Pennings, 1984) studied the effect of adding drops of silicon oil (about 10 mg) to the sample and the reference pan. The purpose of the silicon oil was to provide good thermal contact between the sample and pan to ensure even heating throughout the sample.

In our studies, surgical scissors were used to carefully cut a small piece of melt blown web to fit the sample pan. A sample lid was crimped on the pan to hold the sample in place and improve heat transfer. Silicon oil addition was tested, but its use was discontinued because no change in DSC results occurred when oil was used.

Figure 21 shows a typical DSC scan of melt-blown polypro-

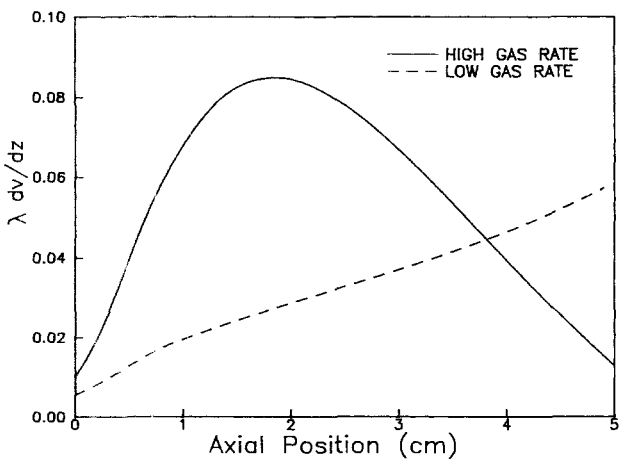

Figure 20. Product $(\lambda)(dv_{fz}/dz)$ vs. axial position.
Calculations were done with the Phan-Thien model, $\beta = 0.60$, and a 5-cm freeze point.

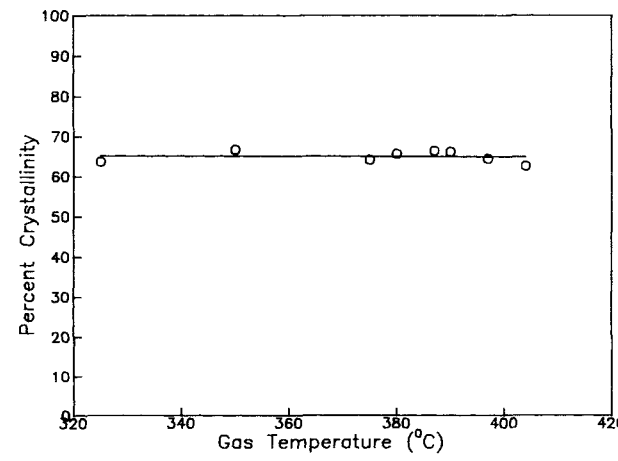

Figure 22. Effect of gas temperature on the crystallinity of melt-blown fibers.
The run conditions were: polymer temperature = 290°C; gas velocity = 150 m/s; polymer flow rate = 3.30 mm³/s.

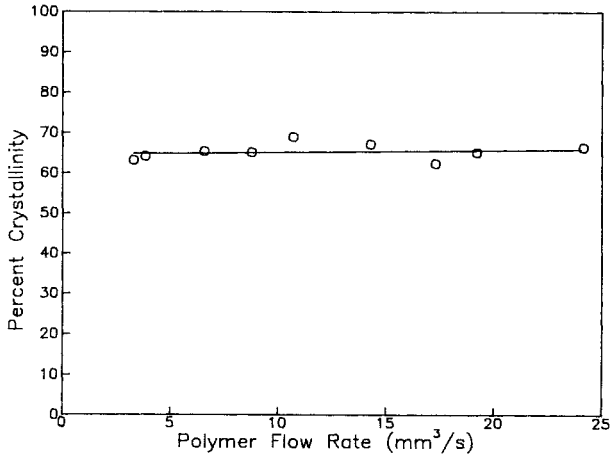

Figure 23. Effect of polymer flow rate on crystallinity.
The run conditions were as follows: polymer temperature = 290°C; gas velocity = 150 m/s; gas temperature = 400°C.

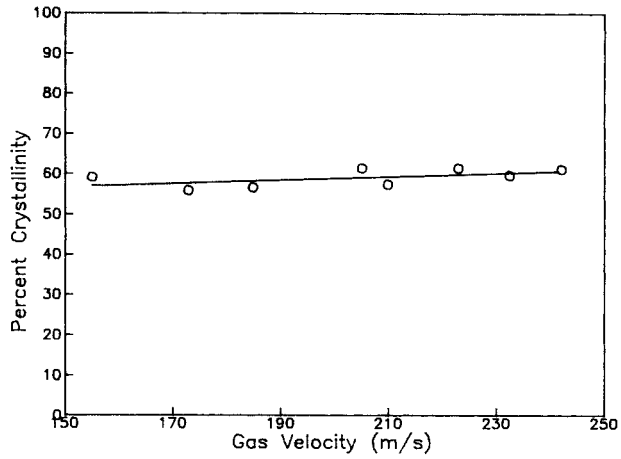

Figure 25. Effect of gas velocity on crystallinity.
The run conditions were as follows: polymer temperature = 290°C; gas temperature = 400°C; polymer flow rate = 3.30 mm³/s.

pylene. A very small endothermic peak occurs at about 120°C. Fichera and Zannetti (1975) and De Candia et al. (1987) also observed a peak of this type during DSC analysis of isotactic polypropylene. Fichera and Zannetti attributed this peak to the melting of crystalline regions formed by annealing. A single main peak at about 159°C occurs on the DSC trace. Because of our high spinning speed and relatively low polymer MFR (melt flow rate) of 35, this single peak is undoubtedly due to a monoclinic crystal structure (Lu and Spruiell, 1987; Shimizu et al., 1979).

The percent crystallinity of the melt blown samples was determined by the commonly used relation (Dole, 1967)

$$\% \text{ crystallinity} = \frac{\Delta H_f}{\Delta H_o} \cdot 100$$

where ΔH_f is the heat of fusion of the sample and ΔH_o is the heat of fusion of 100% crystalline material. A value of 146.5 J/gm was assumed for ΔH_o (Huda, 1985).

Polypropylene was melt blown over wide ranges of the four major operating parameters: polymer flow rate, polymer temperature, gas flow rate, and gas temperature. The melt blown samples were then analyzed for percent crystallinity by DSC. The results of these runs are shown in Figures 22 to 25. The data show fiber crystallinities that average about 62%. These crystallinities compare well with crystallinities of 50 to 65% (by density measurements) that were determined by Lu and Spruiell (1987) for as-spun 35 MFR polypropylene processed at spinning speeds of 1,300 to 5,700 m/min.

In spite of the fact that Figures 22 to 25 cover wide operating ranges, there are no definitive trends in crystallinity as a function of the operating parameters. One explanation for this is that the crystallinity levels in melt blowing are in a plateau region of operation. Another possible explanation relates to the fact that, after solidification, the melt-blown fiber continues to be exposed to the hot melt blowing gas. Perhaps this exposure tends to even out the thermal character of the fibers; the "annealing" peak at 120°C may be evidence of this exposure.

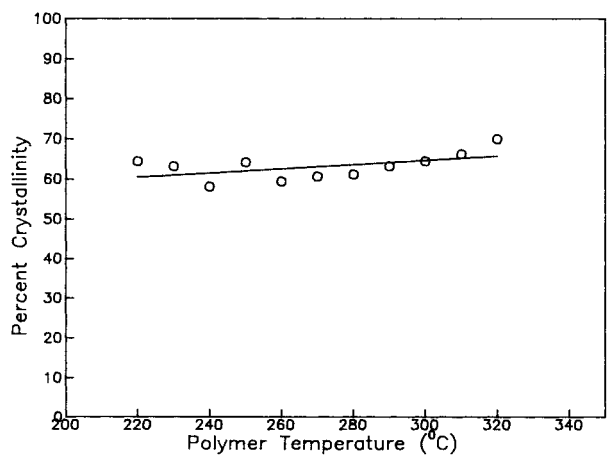

Figure 24. Effect of polymer temperature on crystallinity.
The run conditions were as follows: gas velocity = 150 m/s; gas temperature = 400°C; polymer flow rate = 3.30 mm³/s.

Conclusions

In the modeling of the melt-blowing process, the dependence of the viscosity on temperature is of primary importance, while the choice of constitutive equation is secondary.

Though the exact filament freeze temperature is not known, the model calculations imply that stress-induced crystallization or a similar phenomenon causes a substantial increase in the effective freeze temperature.

The melt-blowing model described herein provides excellent predictions of fiber profile in the region of high fiber attenuation. However, predictions of final fiber diameters are high. One explanation for this is that, at distances far from the spinneret (e.g., at distances greater than 5 to 10 cm, depending on experimental conditions), the filament is observed to exhibit a slight wavering or vibration. As the filament moves transverse to the air field, the drag on the filament is substantially increased, and the filament is attenuated to a greater extent.

Acknowledgment

The authors wish to thank Tien Wu, John Kayser, Larry Crynes, and Seema Vad for their assistance in this project. The authors are also most

grateful for the financial support provided by the following companies: 3M, Dow, Fina, Johnson & Johnson, Kuraray (Japan), and Phillips Petroleum.

Notation

A = cross-sectional area, m^2
C_f = friction factor at filament-air interface
C_p = isobaric specific heat capacity, J/kg · K
d = diameter, m
E = Phan-Thien and Tanner model parameter related to stress saturation at high extension rates
F = force, N
g = gravitational acceleration constant, m/s^2
G = shear modulus, Pa
h = heat transfer coefficient, $W/m^2 \cdot K$
j = sign carrier of the air drag force in the momentum balance equation
= $+1$ if $v_{az} < v_{fz}$
= -1 if $v_{az} \geq v_{fz}$
k = thermal conductivity, W/m · K
K_i = Phan-Thien and Tanner model variable
K = $\exp[(E/G_i)(2\tau_i^{xx} + \tau_i^{zz})]$
m = exponent in the Kase-Matsuo correlation
n = exponent in the Matsui correlation
Nu_z = Nusselt number for air
= $(h_z d_z)/(k_{az})$
Q = polymer flow rate, m^3/s
R = gas constant
Re_{rel} = relative Reynolds number
= $(d_z|v_{rel}|)/(\nu_{az})$
T = temperature, K
v = velocity, m/s
X = Phan-Thien and Tanner model parameter related to viscous shear thinning
z = axial coordinate, m

Greek letters

β = proportionality factor in the Matsui correlation
γ = proportionality factor in the Kase-Matsuo correlation
η = dynamic shear viscosity, Pa · s
$[\eta]$ = intrinsic viscosity
λ = stress relaxation time, s
ν = kinematic viscosity, m^2/s
ρ = density, kg/m^3
τ = extra stress, Pa

Subscripts

a = air
i = summation index
f = filament
rel = relative
z = axial position
o = origin of the analysis region

Superscripts

x = coordinate in transverse direction
z = coordinate in spinning direction

Literature Cited

Buntin, R. R., J. P. Keller, and J. W. Harding, "Nonwoven mats by melt blowing," U.S. Patent #3,849,241 (Nov. 19, 1974).

Cooper, S. D., American Petrofina, Deer Park, TX, private communication (1987).

Chung, T. S., and S. Abdalla, "Mathematical Modeling of Air-Drag Spinning for Nonwoven Fabrics," *Polym. Plast. Technol. Eng.*, **24,** 117 (1985).

Clements, J., G. Capaccio, and I. M. Ward, "Melting Behavior of Ultra-high Modulus Linear Polyethylene," *J. Polym. Sci. Polym. Phys. Ed.*, **7,** 693 (1979).

De Candia, F., R. Russo, and V. Vittoria, "Mechanical Behavior of Quenched Isotactic Polypropylene Crystallized by Thermal and Solvent Treatments," *J. Appl. Polym. Sci.*, **34,** 689 (1987).

Dole, M., "Crystallinity from Thermal Measurements," *J. Polym. Sci.*, **C-18,** 57 (1967).

Fichera, A., and R. Zannetti, "Thermal Properties of it-Polypropylene from the Melt and Annealed," *Die Makromolekulare Chemie,* **176,** 1885 (1975).

Fisher, R. J., and M. M. Denn, "A Theory of Isothermal Melt Spinning and Draw Resonance," *AIChE J.*, **22**(6), 236 (1976).

Gagon, D. K., and M. M. Denn, "Computer Simulation of Steady Polymer Melt Spinning," *Polym. Eng. Sci.*, **21,** 844 (1981).

Huda, M. Nurul, H. Dragaum, S. Bauer, H. Mushik, and P. Skalicky, "A Study of the Crystallinity Index of Polypropylene Fibres," *Coll. Polym. Sci.*, **263,** 730 (1985).

Jaffe, M., "Fibers," Chap. 7, p. 721, *Thermal Characterization of Polymeric Materials,* E. A. Turi, ed., Academic Press, Orlando, FL (1981).

Ishizuka, O., K. Koyama, and H. Nokubo, "Elongational Viscosity in the Isothermal Melt Spinning of Polypropylene," *Polym.* **21,** 691 (1980).

Kase, S., and T. Matsuo, "Studies on Melt Spinning. I. Fundamental Equations on the Dynamics of Melt Spinning," *J. Polym. Sci.*, **A-3,** 2541 (1965).

Lu, F., and J. E. Spruiell, "The Influence of Resin Characteristics on the High Speed Spinning of Isotactic Polypropylene: I. Effect of Molecular Weight and its Distribution on Structure and Mechanical Properties of as-spun Filaments," *J. Appl. Polym. Sci.*, **34,** 1521 (1987).

Matovich, M. A., and J. R. A. Pearson, "Spinning a Molten Threadline: Steady State Isothermal Viscous Flows," *Ind. Eng. Chem. Fund.*, **8**(3), 512 (1969).

Matsui, M., "Air Drag on a Continuous Filament in Melt Spinning," *Trans. Soc. Rheol.*, **20**(3), 465 (1976).

McAmish, L. H., T. O. Addy, and G. F. Lee, "Nonwoven Medical Fabric," U.S. Patent #4,622,259 (Nov. 11, 1986).

Middleman, S., *Fundamentals of Polymer Processing,* McGraw-Hill, New York (1977).

Narasimhan, K. M., and R. L. Shambaugh, "Fiber/Gas Interaction During Melt Blowing," Society of Rheology Meeting, Tulsa, OK (1986).

Narasimhan, K. M., and R. L. Shambaugh, "The Melt Blowing of Polyolefins," Society of Rheology Meeting, Atlanta (1987).

Papanastasiou, T. C., C. W. Macosko, L. E. Scriven, and Zhao Chen, "Fiber Spinning of Viscoelastic Liquid," *AIChE J.*, **33**(5), 834 (1987).

Petrie, C. J. S., *Elongational Flows,* Pitman, London (1979).

Phan-Thien, N., "A Nonlinear Network Viscoelastic Model," *J. Rheol.*, **22**(3), 259 (1978).

Schultz, W. W., "Slender Viscoelastic Fiber Flow," *J. Rheol.*, **31,** 733 (1987).

Schwarz, E. C. A., "Apparatus and Process for Melt Blowing a Fiber-forming Thermoplastic Polymer and Product Produced Thereby," U.S. Patent #4,380,570 (Apr. 19, 1983).

Shambaugh, R. L., "A Macroscopic View of the Melt-Blowing Process for Producing Microfibers," *Ind. Eng. Chem. Res.*, **27**(12), 2363 (1988).

Shimizu, J., N. Okui, and Y. Imai, *Sen-i Gakkaishi,* **35,** T-405 (1979).

Smook, J., and J. Pennings, "Influence of Draw Ratio on Morphological and Structural Changes in Hot-Drawing of UHMW Polyethylene Fibres as Revealed by DSC," *Coll. Polym. Sci.*, **262**(9), 712 (1984).

Tadmor, Z., and C. G. Gogos, *Principles of Polymer Processing,* Wiley, New York (1979).

Tzoganakis, C., J. Vlachopoulos, and A. E. Hamielec, "Production of Controlled-Rheology Polypropylene Resins by Peroxide Promoted Degradation During Extrusion," *Polym. Eng. Sci.*, **28,** 170 (1988).

Van Krevelin, D. W., and P. J. Hoftyzer, *Properties of Polymers—Correlations with Chemical Structure,* Elsevier, New York, 1976.

Wente, V. A., "Manufacture of Superfine Organic Fibers," U.S. Department of Commerce, Office of Technical Services Report No. PB111437, NRL-4364 (Apr. 15, 1954).

———, "Superfine Thermoplastic Fibers," *Ind. Eng. Chem.*, **48,** 1342 (1956).

Ziabicki, A., *Fundamentals of Fibre Formation,* Wiley, New York (1976).

Ziabicki, A., and H. Kawai, eds., *High-Speed Fiber Spinning: Science and Engineering Aspects*, Wiley, New York (1985).
Ziabicki, A., and K. Kedzierska, "Mechanical Aspects of Fibre Spinning Process in Molten Polymers: 1. Stream Diameter and Velocity Distribution Along the Spinning Way," *Kolloid-Z*, **171**, 51 (1960).
———, "Mechanical Aspects of Fibre Spinning Process in Molten Polymers: 2. Stream Broadening after the Exit from the Channel of Spinneret," *Kolloid-Z*, **171**, 111 (1961).
Ziabicki, A., "Mechanical Aspects of Fibre Spinning Process in Molten Polymers: 3. Tensile Force and Stress," *Kolloid-Z*, **175**, 14 (1961).

Manuscript received Mar. 13, 1989, and revision received Nov. 13, 1989.